Utilising energy transfer in binary and ternary bulk heterojunction organic solar cells

Krishna Feron[a,b,*], James M. Cave[c], Mahir N. Thameel[b,d], Connor O'Sullivan[b], Renee Kroon[e,f], Mats R. Andersson[e,f], Xiaojing Zhou[b], Christopher J. Fell[a], Warwick J. Belcher[b], Alison B. Walker[c], Paul C. Dastoor[b]

[a] CSIRO Energy, Newcastle, NSW 2300, Australia

[b] Centre for Organic Electronics, University of Newcastle, University Drive, Callaghan, NSW, 2308, Australia

[c] Department of Physics, University of Bath, Bath BA2 7AY, United Kingdom

[d] Department of Physics, College of education for pure science, University of Anbar, Iraq

[e] Future Industries Institute, University of South Australia, Mawson Lakes Campus, SA 5095, Australia

[f] Department of Chemistry and Chemical Engineering/Polymer Technology, Chalmers University of Technology, 41296 Göteborg, Sweden

*Corresponding author, e-mail: Krishna.Feron@csiro.au

Abstract

Energy transfer has been identified as an important process in ternary organic solar cells. Here, we develop kinetic Monte Carlo (KMC) models to assess the impact of energy transfer in ternary and binary bulk heterojunction systems. We used fluorescence and absorption spectroscopy to determine the energy disorder and Förster radii for poly(3-hexylthiophene-2,5-diyl), [6,6]-Phenyl-C61-butyric acid methyl ester, 4-bis[4-(N,N-diisobutylamino)-2,6-dihydroxyphenyl] squaraine (DIBSq) and poly(2,5-thiophene-alt-4,9-bis(2-hexyldecyl)-4,9-dihydrodithieno[3,2-c:3′,2′-h][1,5]naphthyridine-5,10-dione). Hetero-energy transfer is found to be crucial in the exciton dissociation process of both binary and ternary organic semiconductor systems. Circumstances favouring energy transfer across

interfaces allow relaxation of the electronic energy level requirements, meaning that a cascade structure is not required for efficient ternary organic solar cells. We explain how energy transfer can be exploited to eliminate additional energy losses in ternary bulk heterojunction solar cells, thus increasing their open-circuit voltage without loss in short-circuit current. In particular, we show that it is important that the DIBSq is located at the electron donor/acceptor interface, otherwise charge carriers will be trapped in the DIBSq domain or excitons in the DIBSq domains will not be able to dissociate efficiently at an interface. KMC modelling shows that only small amounts of DIBSq (<5% by weight) are needed to achieve substantial performance improvements due to long-range energy transfer.

Keywords

Ternary organic solar cells; binary photovoltaic; energy transfer; exciton dissociation; Monte Carlo; energy level optimization

1. Introduction

The power conversion efficiency (PCE) of organic solar cells (OSCs) has consistently improved over the last 2-3 decades as a result of our increased understanding of the photoconversion mechanism in these devices[1]. In organic semiconductors, tightly bound excited states (excitons) are created upon light absorption[2]. These quasi-particles can be dissociated using a sufficiently large electrochemical potential at a heterojunction to create a charge-transfer (CT) state. The CT state may either recombine or result in separated charge carriers. The driving force required to efficiently convert excitons into separated charge carriers is seen to be at least 0.6 eV[3,4]. This rather large energy sacrifice reduces the open-circuit voltage (V_{OC}) significantly and is the most important reason why organic solar cells are less efficient than inorganic solar cells[5].

Binary organic semiconductor systems have been the primary focus of OSC research over the last three decades. However, the last couple of years has seen a large interest in ternary semiconductor

systems[6–10] or even quaternary systems[11]. In general, ternary solar cells consist of a polymer as the host electron donor, a fullerene derivative as the host electron acceptor and a third species as an infra-red sensitizer. Provided the absorption spectra of the different types of organic molecules complement each other, ternary systems are expected to absorb more light and thus achieve higher PCE than equivalent binary systems. In addition, the infra-red sensitiser is also observed to affect the microstructure of the photoactive layer[7,8,12]. Generally, only small amounts of the infrared sensitizer (<5 % by weight) are already observed to change the microstructure resulting in improved fill factor (FF) (indicative of reduced bimolecular recombination)[8]. Successful ternary bulk heterojunction (BHJ) structures often use materials where the third absorber is situated at the donor:acceptor interface (driven by surface energy)[8,12]. These observations suggest that the optimum relative concentration and highest PCE are determined by morphological constraints and, to a lesser extent, by light harvesting. In order to explain the experimental observations in ternary devices, a modelling approach that takes into account the complex ternary morphology is required. Kinetic Monte Carlo models have already been developed to investigate complex morphologies in binary BHJ systems[13–17] and offer an ideal modelling approach to also investigate ternary bulk heterojunction structures.

Due to the addition of another electronically active component, ternary solar cells operate via a more complicated mechanism. In general, there are three photoconversion mechanisms in ternary organic photovoltaic (OPV) devices which are not mutually exclusive: (i) cascade charge transfer, (ii) energy transfer, (iii) parallel-like charge transfer[10]. These mechanisms are depicted in Figure 1. Cascade charge transfer relies on the energy levels to form a cascade structure, so that electrons and holes can hop between all three materials and excitons can dissociate at each interface. Mechanism (i) places restrictions on the lowest and highest occupied molecular orbitals (LUMO and HOMO) of all three materials and thus limits the number of materials that can be combined to form a ternary cascade charge transfer system. Mechanism (ii) relies on energy transfer to move the exciton from one component to another component with a smaller optical gap. Such energy transfer has been observed to occur over relatively large distances (>20 nm)[9]. Once transferred, the exciton simply

follows the same mechanism as it would in a binary device. While the absorption and fluorescence spectra of the energy acceptor and donor must overlap, there are no restrictions on the position of the HOMO and LUMO. Furthermore, the energy donor is not required to conduct charge carriers provided that the energy donor concentration is low, thus relaxing some of the constraints on materials choice. In mechanism (iii) ternary devices are thought to act as two binary devices, meaning that there are either two electron donors with just one electron acceptor or two electron acceptors with just one donor. There is no charge or energy transfer between two of the three components.

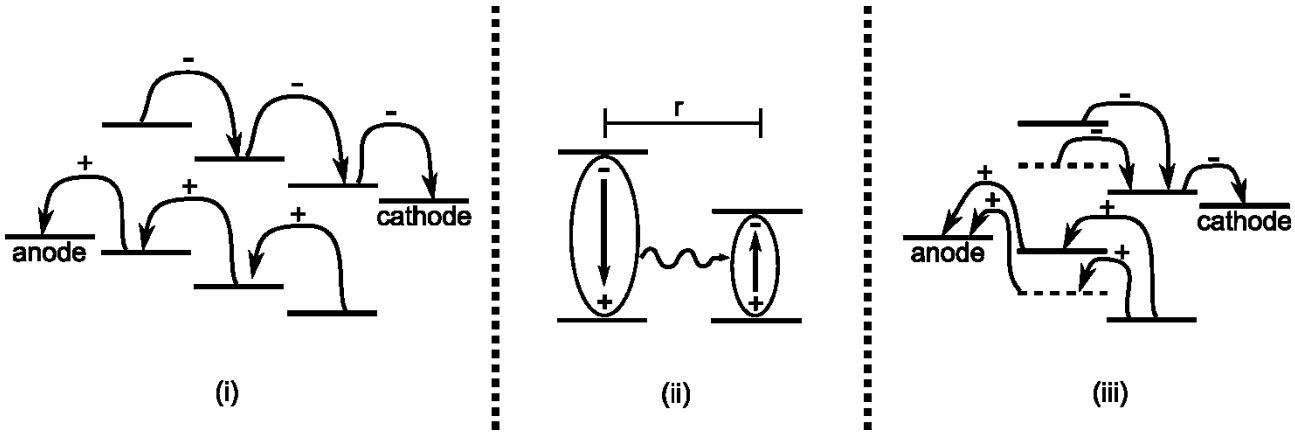

Figure 1. Three mechanisms that are relevant to ternary organic solar cells: (i) cascade charge transfer, (ii) energy transfer across a distance *r*, (iii) parallel-like charge transfer

Irrespective of the type of photoconversion mechanism that is at play, the absorption spectra of the three materials are chosen to be complementary. Consequently, it is almost certain that the fluorescence spectrum of one material has overlap with the absorption spectrum of another. In other words, energy transfer is expected to occur to some extent in all ternary devices[18].

Energy transfer has been identified in poly(3-hexylthiophene-2,5-diyl) : [6,6]-Phenyl-C61-butyric acid methyl ester : 4-bis[4-(N,N-diisobutylamino)-2,6-dihydroxyphenyl] squaraine (P3HT:PCBM:DIBSq) ternary devices[8]. While the ternary blend was shown to perform better than the binary equivalent, it is not clear how important energy transfer is to the success of this particular ternary blend. For example, quantification of what fraction of excitons is affected by energy transfer is current lacking. While this information would aid in assessing whether efficient energy transfer is

required or is rather a side-effect with little impact on overall device efficiency, it is difficult to quantify this contribution experimentally. Instead, a rigorous modelling effort is required to investigate the importance of energy transfer in ternary systems.

In this manuscript we measure absorption and fluorescence spectra to determine the energy transfer parameters for P3HT, PCBM, poly(2,5-thiophene-alt-4,9-bis(2-hexyldecyl)-4,9-dihydrodithieno[3,2-c:3′,2′-h][1,5]naphthyridine-5,10-dione) (PTNT) and DIBSq. A kinetic Monte Carlo (KMC) model is developed for binary and ternary BHJ systems to investigate energy transfer and exciton dissociation. Firstly, we assess the impact of energy transfer on the exciton dissociation processes in P3HT:PCBM BHJ blends and we show that energy transfer is significant even in binary devices. The KMC model is also applied to two ternary BHJ blend systems: the popular P3HT:PCBM:DIBSq[8,19] and PTNT:PCBM:DIBSq. PTNT has similar optical properties to P3HT, but a different energy level offset, thus providing an ideal comparison for exploring the effect of the energy level offset at the heterojunction on device performance. Importantly, we show that the energy sacrifice required for efficient charge separation can be drastically reduced by utilising energy transfer in ternary blends, thus providing a pathway towards increasing the V_{OC} in ternary organic solar cells.

2. Simulation and Experimental Methodology

2.1 Förster resonance energy transfer theory

One of the primary energy transfer mechanisms in OPV devices is Förster Resonance Energy Transfer (FRET) and is generally used in KMC models[13,14,18,20,21]. FRET is a form of non-radiative energy transfer, where no real photon is emitted or absorbed. An exciton localised on one molecule (the donor) acts as an oscillating dipole and can couple to an electron in the ground state on another molecule (the acceptor) – the energy of the exciton is transferred to the electron in the ground state, producing an exciton at the new position. The exciton appears to instantaneously 'hop' from one place to another. The rate of transfer is given by[22]

$$k_{FRET} = \frac{1}{\tau}\left(\frac{R_0}{r}\right)^6 \quad (1)$$

where τ is the lifetime of the exciton in the absence of any possible acceptor sites, r is the distance between the exciton and the acceptor site in question and R_0 is the Förster radius between the two materials. The Förster radius is the distance at which the rate of recombination, $1/\tau$, and rate of transfer, k_{FRET}, are equal and is given by:

$$R_0^6 = \frac{9000\, Q_0 (\ln 10) \kappa^2\, J}{128\, \pi^5 n^4 N_A} \tag{2}$$

where Q_0 is the fluorescence quantum yield, κ the orientation factor, n the refractive index, N_A Avogadro's number and J the overlap integral, which is given by

$$J = \int_0^\infty F_D \epsilon_A \lambda^4 d\lambda \tag{3}$$

where λ is the wavelength of light, F_D is the fluorescence spectrum of the energy donor normalised so that $\int_0^\infty F_D d\lambda = 1$, and ϵ_A the molar extinction coefficient of the energy acceptor. Förster theory ignores solid-state interactions and only considers the interaction between isolated dipoles (molecules). As such, it is more appropriate to use the optical properties of materials as measured in solution as opposed to in the solid-state. Moreover, the absorbance of DIBSq in a ternary blend film closely resembles that of DIBSq in solution and does not match the absorbance of a DIBSq solid film (see Supporting Information). κ is given by[23]

$$\kappa = \overrightarrow{u_D} \cdot \overrightarrow{u_A} - 3(\vec{r} \cdot \overrightarrow{u_D})(\vec{r} \cdot \overrightarrow{u_D}) \tag{4}$$

Where $\overrightarrow{u_D}$ and $\overrightarrow{u_A}$ are the unit vectors of the energy donor and acceptor dipoles respectively, and $\vec{r}$ is the unit vector between the two dipoles. If the donor site and the acceptor site are of the same material, this process is known as homo-energy transfer, otherwise the hop is referred to as hetero-energy transfer.

2.2 Kinetic Monte Carlo model

The kinetic, or dynamic, Monte Carlo (KMC) method is a stochastic algorithm for simulating the evolution of a system over time. For a given set of events and knowledge of (or a way to calculate) the rates at which they occur, a KMC simulation provides trajectories of the individual entities in the system. As such, the simulation is a useful tool for our purposes, as we can see the fraction of excitons

that, for example, hop across an interface before dissociating. In our system, possible events include: (i) excitons hopping from one lattice site to another via homo- or hetero-energy transfer, (ii) an exciton recombining on its current lattice site, (iii) an exciton dissociating across a boundary from its present site to an adjacent site of a different material and, (iv) a new exciton being generated on an empty site.

Here, we use the First Reaction Method (FRM) approach for the KMC model[24]. At the start of the simulation, the time, t_i, for each possible event i to occur is calculated according to the formula

$$t_i = -\left(\frac{1}{r_i}\right) \ln u \tag{5}$$

where r_i is the rate at which i occurs and u is a uniformly drawn random number in the range (0, 1]. The negative natural logarithm of a uniform random number produces random numbers from an exponential distribution (suitable for times between events in a Poisson process) and dividing by the rate appropriately scales the distribution so that a faster rate leads to shorter times. Events with slower rates can occur sooner than those with faster rates (as a consequence of the random number generation) but overall events will occur as often as would be expected statistically.

Events are then entered into the central queue; a chronologically ordered list of all the events which may occur in the system. Events are executed from the list sequentially, starting with the event with the shortest time, and each time an event occurs its time to occur is subtracted from all other queue members and any newly enabled events determined and entered into the queue.

The occurrence of some events may invalidate other events. For example, if an exciton recombines it can no longer make a FRET hop. As such, the validity of each event is checked before it is executed, and if the event has become invalidated it is removed from the queue without execution. In the case of mutually exclusive events, only the event with the shortest time need be inserted as it will necessarily be executed first. After the execution of an event, any newly enabled events are calculated with a time to occur given by Equation 5 and added to the queue in the appropriate position to maintain temporal order. For example, after a generation event the newly generated exciton will have a hop event and a recombination event inserted into the queue.

In our system, we consider a cubic lattice of hopping sites with lattice spacing of 1 nm, and site occupancy that is limited to one exciton at a time. All FRET hops between an exciton's current site and every other site within 30 nm are calculated. The temperature of the system is 300 K. Periodic boundary conditions exist for all three dimensions. The excitonic energies on each lattice site are randomly drawn from a Gaussian distribution at the start of each run, with a standard deviation given by the energy disorder of the material as calculated by fitting a Gaussian to the absorption spectrum of each material[14].

Thermally activated hopping rates, k_{ET}, are calculated via

$$k_{ET} = \frac{1}{\tau}\left(\frac{R_0}{r}\right)^6 \times \begin{cases} 1 & \Delta E \leq 0 \\ \exp\left(-\frac{\Delta E}{k_B T}\right) & \Delta E > 0 \end{cases} \quad (6)$$

where τ is the exciton lifetime for the current site, R_0 the Förster radius between the current and final site materials, r the distance between sites, ΔE the change in energy, k_B the Boltzmann constant and T the absolute temperature of the system. The Boltzmann multiplier for $\Delta E>0$ reduces the rate of hops which result in an increase in energy. The recombination rate of an exciton is simply the inverse of its lifetime in its current material,

$$k_{recomb} = \frac{1}{\tau}. \quad (7)$$

Exciton generation is calculated for the entire system, with a global rate

$$k_{gen} = gN, \quad (8)$$

where N is the total number of lattice sites in the system and g the generation rate per lattice site. In order to draw general conclusions about energy transfer mechanisms, the same generation rate is used for all materials. A value for g of 10 excitons per second per lattice site was found to approximate to 1000 W/m^2 illumination under the AM1.5 standard spectrum. After each generation event, a new exciton is placed at a random unoccupied site on the lattice.

Exciton dissociation is handled separately from the event system; when an exciton is created on, or hops to, a site of some material adjacent to a site of a different material (an interface site), it has a chance to dissociate with some probability, p. The exciton either dissociates instantly across the

interface or does nothing. If it does not dissociate, it can gain more chances to dissociate at the same or another interface by hopping to more interface sites; it can also hop back to previous interface sites it has visited to obtain more chances there. The probability p can be different for an exciton depending on which side of the interface it resides. For example, p may be different on the P3HT side of a P3HT:PCBM interface than on the PCBM side as the former proceeds via electron transfer and the latter via hole transfer.

3D BHJ morphologies were created following a cellular automata method previously described[14].

2.3 Materials

P3HT was synthesised in-house, PCBM was purchased from Solenne, Rhodamine 6G (R6G) and DIBSq were purchased from Sigma Aldrich, and PTNT was synthesised in-house as previously described[25]. All materials were used as received. The chemical structures are shown in Figure 2.

2.4 Spectroscopy

Absorption spectra of the materials were measured in solution using a Cary Varian 6000i. Fluorescence spectra were measured in solution using a Cary Eclipse fluorimeter. The fluorescence quantum efficiency, Q_0, was determined using a rhodamine 6G standard (95 % fluorescence quantum efficiency in ethanol) following a standard procedure [26].

The HOMO levels of P3HT, PCBM, DIBSq and PTNT were measured using a Riken Keiki AC2 photoelectron spectroscopy in air (PESA) setup. The LUMO levels were found by adding the optical band gap to the measured HOMO. The optical band gap was determined by finding the intersection of the absorption baseline with a straight line fitted to the steepest part of the slope near the onset of light absorption.

3. Results and discussion

3.1 Material Parameters

The fluorescence quantum efficiency, exciton diffusion length, L, and exciton lifetime, τ, for all materials and Q_0 for PCBM are taken from literature (reference included in Table 1). Q_0 for P3HT and PCBM were measured. L has not previously been determined for PTNT. Since, the optimal domain size of PTNT:$PC_{70}BM$ blend devices[25] is approximately the same as that of P3HT:PCBM blend devices[27] (both are around 10-20 nm), it is reasonable to assume a similar exciton diffusion length for both PTNT and P3HT. The material properties are summarised in Table 1. The standard deviation of Gaussian energy disorder, σ, was estimated by fitting a Gaussian to the edge of the absorption spectrum[28,29].

Table 1. Q_0, L, τ and σ for P3HT, PCBM and DIBSq

Materials	Q_0 (%)	L (nm)	τ (ns)	σ (eV)
P3HT	25	8.5 [30]	0.9 [19]	0.06
PCBM	8.3 x 10^{-2} [31]	5 [32]	1.43 [31]	0.09
PTNT	32	8.5 [33]	0.9 [34]	0.09
DIBSq	-	2 [35]	4.9 [19]	0.05

The absorption and fluorescence spectra of P3HT, PCBM, DIBSq and PTNT in solution are shown in Figure 2, along with the AM1.5 spectrum. Using the absorption and fluorescence measurements the Förster radius was calculated using equations (2) and (3) for all relevant energy transfer pathways and are summarised in Table 2. The refractive indices, n, were all taken to be 1.4 [8] and the squared dipole orientation factor, κ^2, is taken to be its average value of 2/3 for all transfers (random orientation of dipoles)[18]. Values for the Förster radii within materials, i.e. for homo-energy transfer, were found using the KMC model as follows (Table 2). For each material, a volume element of dimensions 100×100×100 voxels was simulated and a single exciton placed in the centre. Exciton

generation was switched off for these simulations.

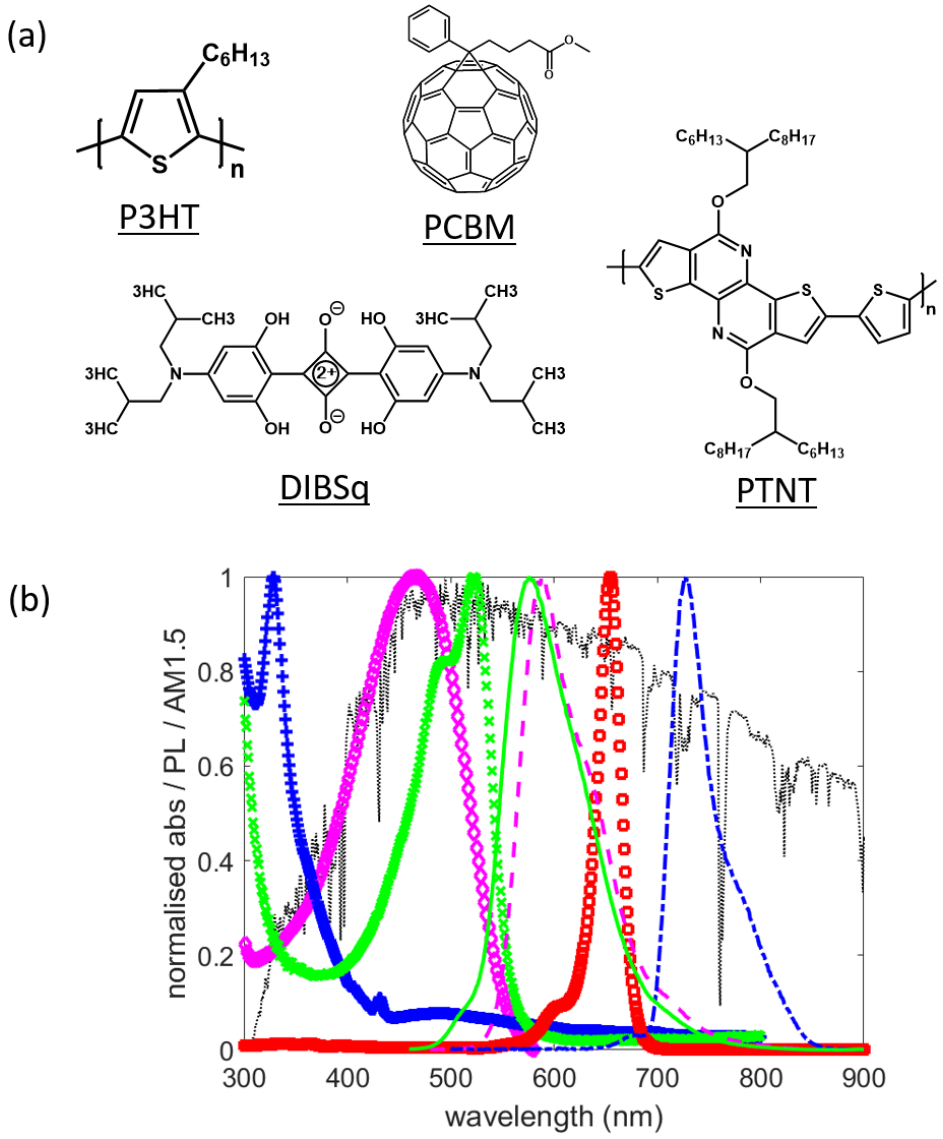

Figure 2. (a) The chemical structures of the materials under study. (b) Normalised absorbance: blue plus signs indicates PCBM, magenta diamonds P3HT, green crosses PTNT and red squares DIBSq. Normalised fluorescence: green solid line indicates PTNT, magenta dashed lines P3HT and blue dash-dot line PCBM. The normalised AM1.5 is shown as a black dotted line.

The exciton was allowed to hop around the system until it recombined, at which point the total displacement was recorded and the system reset with a new randomised energy landscape and run again. The diffusion length in the material is taken to be the root-mean-square of the set of distances travelled. For a given material with a known energy disorder, σ, and exciton lifetime, τ, the diffusion

length of the exciton in the material is dependent only on the (homo-energy transfer) Förster radius. R_0 was chosen such that the calculated diffusion length for each material agreed with the corresponding value in Table 1.

Table 2. Förster radii for all relevant energy transfer combinations.

R_0 (nm)		**Energy acceptor**			
		P3HT	**PTNT**	**PCBM**	**DIBSq**
Energy donor	**P3HT**	2.3	-	2.7	5
	PTNT	-	2.3	2.8	5.2
	PCBM	-	-	2.3	1.2
	DIBSq	-	-	-	1.1

3.2 Impact of the dissociation probability and hetero-FRET in a P3HT:PCBM BHJ device

Exciton dissociation is an important process in generating charges in OPV devices. Generally, dissociation is achieved by one of the three processes depicted in Figure 3. In process (i) light is absorbed by a PCBM molecule giving rise to an exciton. This exciton can dissociate efficiently at a P3HT:PCBM interface. The LUMO of P3HT and PCBM are such that electron transfer from PCBM to P3HT is unfavourable, while the HOMO offset allows for efficient hole transfer from PCBM to P3HT. Hence, in process (i) excitons are dissociated via hole transfer only. In process (ii), excitons are created in the P3HT phase, which can dissociate via electron transfer to PCBM at a P3HT:PCBM interface. Experimental evidence shows that exciton dissociation at the P3HT:PCBM heterojunction can also proceed via a two-step process[36]. Excitons generated in P3HT move to PCBM via energy transfer and are then dissociated on the PCBM side of the interface via hole transfer from PCBM to P3HT (Figure 3). Clearly, efficient hetero-energy transfer is crucial for this third dissociation

mechanism.

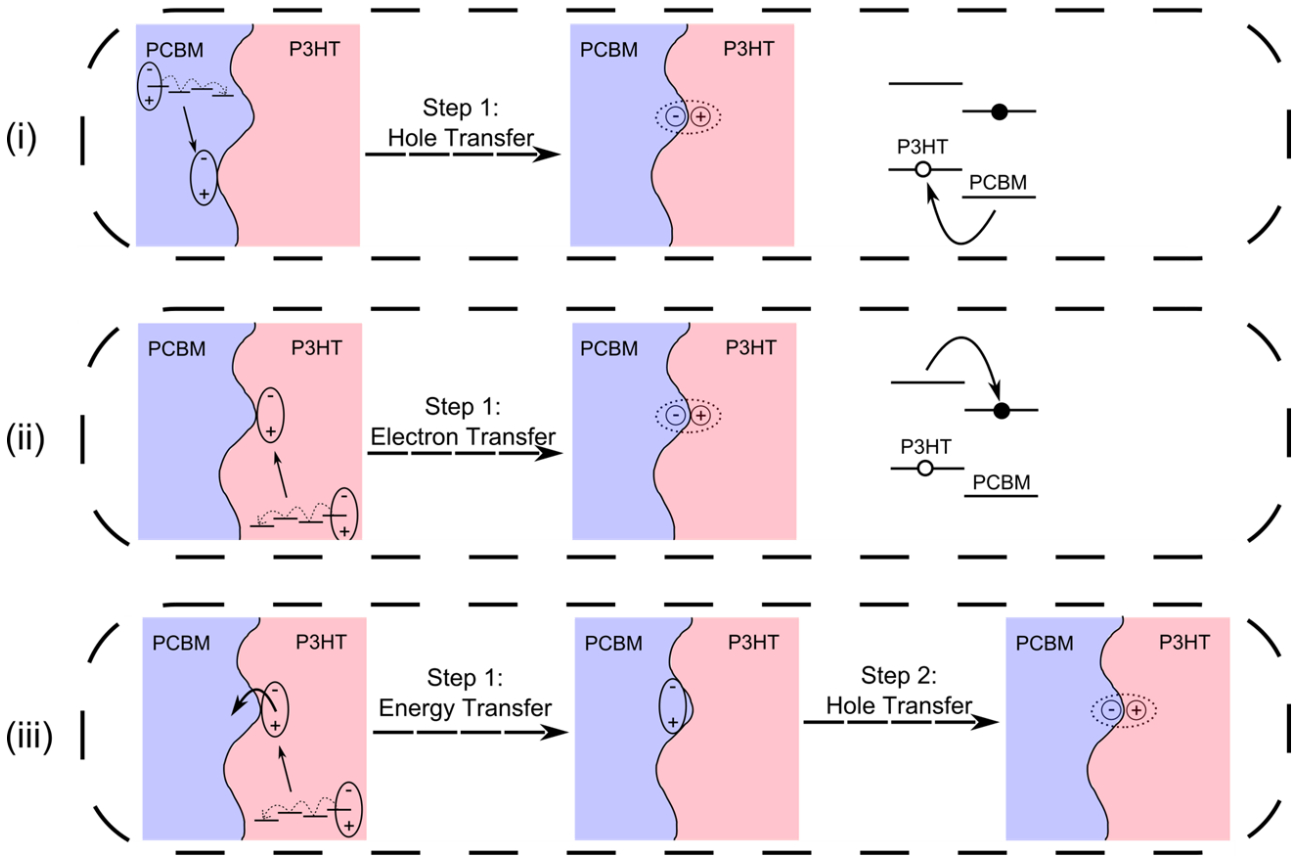

Figure 3. Three dissociation mechanisms in a binary P3HT:PCBM system.

However, hetero-energy transfer is typically ignored when modelling exciton dissociation in binary systems. Here, we investigated the effect of hetero-energy transfer on the exciton dissociation efficiency, *EDE*, which is defined as the fraction of excitons that successfully dissociate. Exciton dissociation can be achieved either by electron transfer (into PCBM) or by hole transfer (into P3HT). The associated driving energy ($LUMO_{PCBM} - LUMO_{P3HT}$ or $HOMO_{P3HT} - HOMO_{PCBM}$) determines the rate of this process[37], which determines the electron and hole transfer probabilities. We modelled a 1:1 P3HT:PCBM BHJ morphology with a feature size, f (f=3V/A, where V is volume and A interfacial area), of 15 nm and varied the probability p of an exciton dissociating from 1% to 100% for each side of the interface; p^{hole} for the PCBM side (hole transfer into P3HT) and $p^{electron}$ for the P3HT side (electron transfer into PCBM). Figure 4 shows the *EDE* as a function of p^{hole} and $p^{electron}$

for two cases: (a) the traditional approach of not considering hetero-energy transfer and (b) including hetero-energy transfer as a possibility in the KMC model.

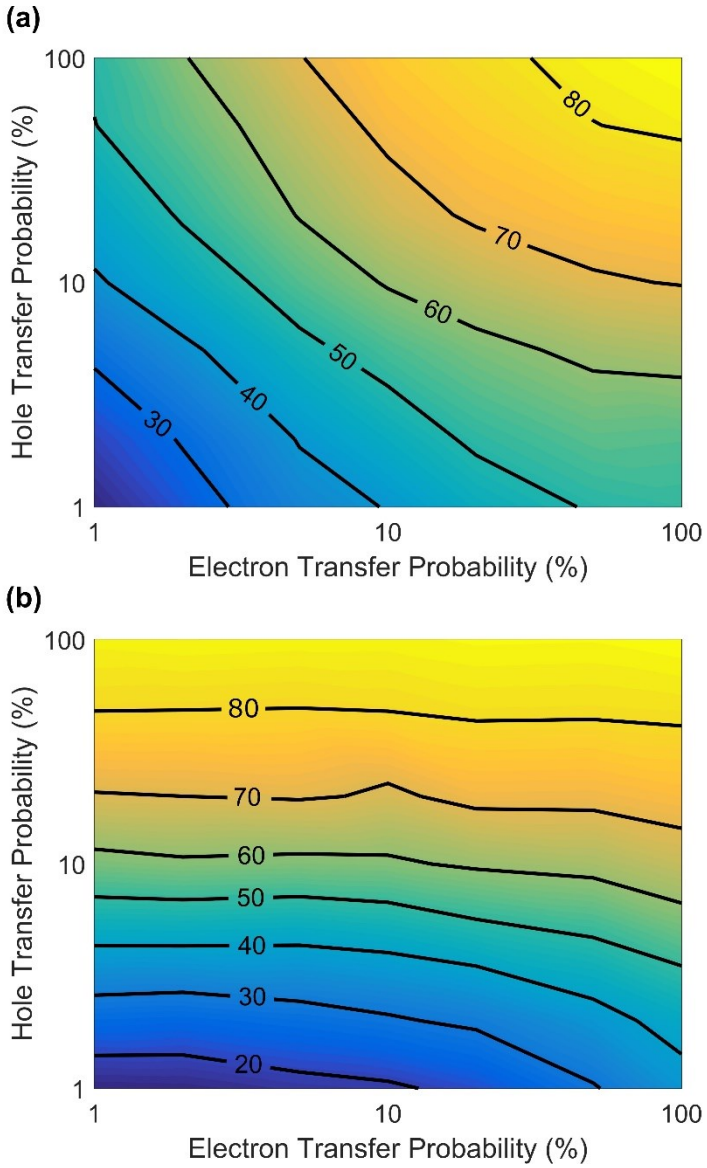

Figure 4. Exciton dissociation efficiency of a BHJ structure with a feature size of 15 nm as a function of p^{hole} and $p^{electron}$ for two cases: (a) not considering hetero-energy transfer and (b) including hetero-energy transfer.

As can be seen from the change in EDE in the vertical direction (hole transfer probability axes) in Figure 4, the hole transfer probability affects *EDE* of the BHJ system very strongly for both cases. The electron transfer probability, on the other hand, does not affect the *EDE* significantly when

hetero-energy transfer is taken into account (Figure 4(b)), because excitons in the P3HT moiety can still dissociate efficiently via the two-step dissociation mechanism even if $p^{electron}$ is small. Lloyd *et al.* measured the external quantum efficiency (EQE) spectrum of P3HT:C_{60} bilayer devices with and without an interlayer that prevented electron transfer from P3HT to C_{60} (i.e. $p^{electron} = 0$) [36]. No change in the EQE spectra was seen when electron transfer from P3HT to C_{60} was prevented, indicating that the *EDE* did not change. The insensitivity of the modelled *EDE* to $p^{electron}$ matches Lloyd *et al.*'s results, further corroborating the two-step dissociation mechanism. When hetero-energy transfer is ignored, p^{hole} and $p^{electron}$ are equally important (Figure 4(b)) and both the driving energies for hole transfer ($HOMO_{P3HT} - HOMO_{PCBM}$) and electron transfer ($LUMO_{PCBM} - LUMO_{P3HT}$) must be optimised. However, since energy transfer between P3HT and PCBM is efficient enough to facilitate the two-step dissociation mechanism, the constraints on the electronic energy levels are relaxed and the electron transfer efficiency from P3HT to PCBM is not limiting.

The difference in EDE for the two cases (with and without hetero-energy transfer) is shown in Figure 5(a). If p^{hole} is similar to $p^{electron}$, the correct *EDE* will be predicted even if hetero-energy transfer is ignored. The dashed line in Figure 5(a) indicates where on the graph the difference in *EDE* is negligible. Only when $p^{hole} \neq p^{electron}$ is it important to consider hetero-energy transfer in binary BHJ blends for calculating *EDE*. It is known that hole transfer is two orders of magnitude faster than electron transfer in P3HT:PCBM blends and that p^{hole} is almost 100 %[38]. We can calculate p^{P3HT} based on the radiative, non-radiative and exciton splitting rates (k_{rad}, k_{nonrad} and k_{split} respectively) using the following equation:

$$p^{P3HT} = \frac{k_{split}}{k_{rad}+k_{nonrad}+k_{split}} \quad (9)$$

Using k_{rad} = 1.67 GHz[38], k_{nonrad} = 5 GHz[39] and k_{split} = 100 GHz[38], $p^{electron}$ is estimated to be approximately 94 %. Since both charge transfer probabilities are very similar, hetero-energy transfer can be ignored for P3HT:PCBM blends without over- or underestimating *EDE*.

Since the band gap of P3HT is larger than that of PCBM, hetero-energy transfer can only occur from P3HT to PCBM and not vice versa. The number of dissociated excitons that undergo the

two-step dissociation mechanism is shown in Figure 5(b) as a fraction of the total number of dissociated excitons that were originally generated in P3HT. As $p^{electron}$ decreases, the number of dissociated excitons that have undergone hetero-energy transfer increases quickly leading to the insensitivity of *EDE* to $p^{electron}$ as seen in Figure 4 (a).

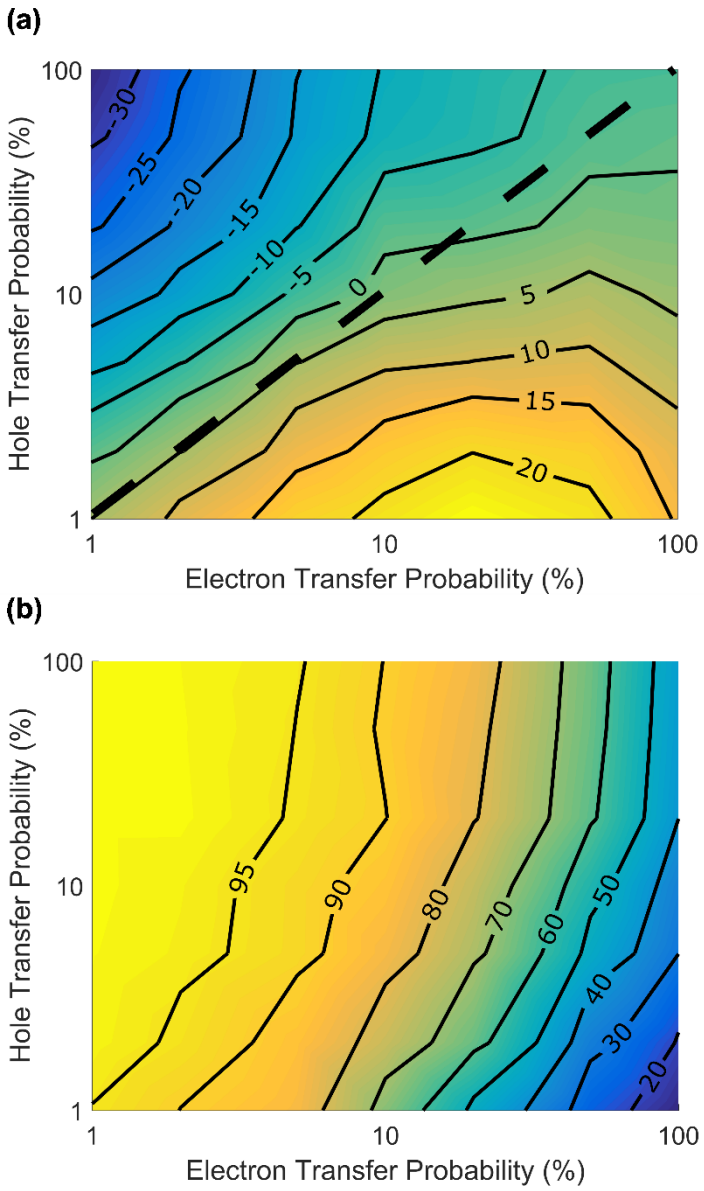

Figure 5. (a) Difference in *EDE* between ignoring and including hetero-energy transfer. The dashed line indicates where the difference in *EDE* is 0. (b) fraction of dissociated P3HT excitons that undergo a two-step exciton dissociation process.

For our expected condition of p^{hole} = 100 % ≈ $p^{electron}$, 43 % of dissociated excitons in P3HT occurs via the two-step mechanism. For low $p^{electron}$ nearly all excitons in P3HT dissociate via the two-step

mechanism. In general, it is important in both binary and ternary systems to consider hetero-energy transfer so that this significant dissociation behaviour is not missed.

3.3 Ternary BHJs

While binary systems only have one type of interface (e.g. P3HT:PCBM) and thus 2 energy offsets to drive exciton dissociation, ternary systems include 3 types of interfaces and 6 energy offsets. Since it is difficult to ensure that all 6 offsets are such that all 6 charge transfer rates are the same, it is crucial to consider hetero-energy transfer in ternary systems to ensure accurate calculation of *EDE*.

The P3HT:PCBM:DIBSq BHJ ternary system has recently received considerable interest [8,19,35,40]. Based on the wetting coefficient of DIBSq in P3HT:PCBM, it is likely that DIBSq is located at the interface between P3HT and PCBM, thus changing the morphology to a more phase-separated structure with crystalline P3HT domains[8]. This surface energy driven phase separation process was also observed for silicon phthalocyanine in P3HT:PCBM[12]. Another indication that DIBSq is located at the P3HT:PCBM interface is to consider the concentration of DIBSq in these blends and the cascade electronic energy structure shown in Figure 6. The experimentally observed optimum DIBSq concentration is less than 5 %, which is far too low to form continuous charge percolation pathways to both electrodes. If DIBSq was located in pure PCBM or P3HT domains, it would simply act as a charge trap, diminishing PV performance and not contributing to photocurrent. However, DIBSq is clearly seen to be photo-active in the EQE spectrum and to improve PV performance[8], which is only possible if DIBSq is able to pass on holes to P3HT and electrons to PCBM. Hence, DIBSq must be in direct simultaneous contact with P3HT and PCBM, i.e. DIBSq must be located at the P3HT:PCBM interface. Following this deduction, virtual P3HT:PCBM:DIBSq BHJ structures were created by placing DIBSq voxels at the P3HT:PCBM interface. P3HT:PCBM BHJ binary structures were taken as a starting point and DIBSq was added until the desired concentration was reached. The available interface area decreases as the feature size increases. For a feature size of 31 nm, less than 15 % DIBSq could be added before the entire P3HT:PCBM interface was covered with DIBSq. Adding

more DIBSq would necessarily mean that either DIBSq is located in P3HT or PCBM domains (where the DIBSq molecules would simply act as charge traps) or that large DIBSq domains are formed. Since the exciton diffusion length in DIBSQ is very small (<2 nm), excitons in DIBSq can only dissociate efficiently if the DIBSq domains are very small. Therefore, it is plausible that the low optimum DIBSq concentration observed in P3HT:PCBM:DIBSq devices may be determined by the limited available P3HT:PCBM surface area in BHJ structures. The cascade electronic structure shown in Figure 6(a) indicates that the exciton is able to dissociate at all 6 interfaces. Consequently, in the KMC model the dissociation probability at these interfaces was set to 100%.

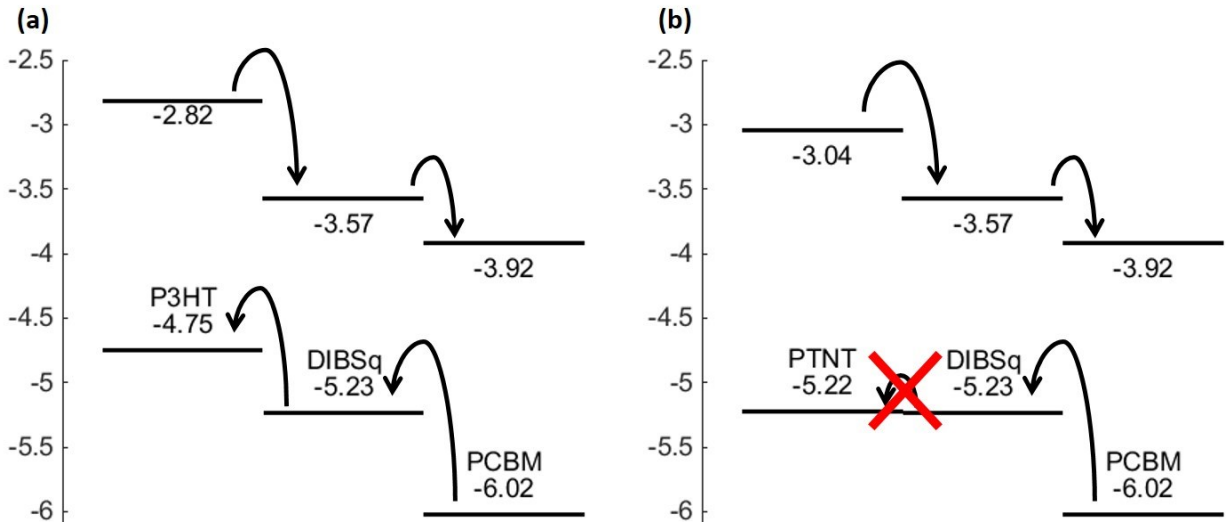

Figure 6. Energy diagram of (a) P3HT, PCBM, DIBSq and (b) PTNT, PCBM, DIBSq. The six charge transfers associated with the six possible ways of splitting the exciton are depicted with arrows. The driving energy is sufficient for efficient exciton dissociation in all but one case: hole transfer across from DIBSq to PTNT is not favourable, because the driving energy of 0.01 eV is less than the exciton binding energy.

Figure 7(a) shows that *EDE* improves significantly in P3HT:PCBM:DIBSq ternary BHJ structures. It is easier for an exciton to find an interface when the feature size is smaller, meaning that *EDE* is naturally larger for these systems and DIBSq has less of an effect. Only a small amount of DIBSq (<5%) is required to effect a substantial increase in *EDE*. While adding more than 5% DIBSq does

continue to improve *EDE*, the rate of improvement decreases significantly.

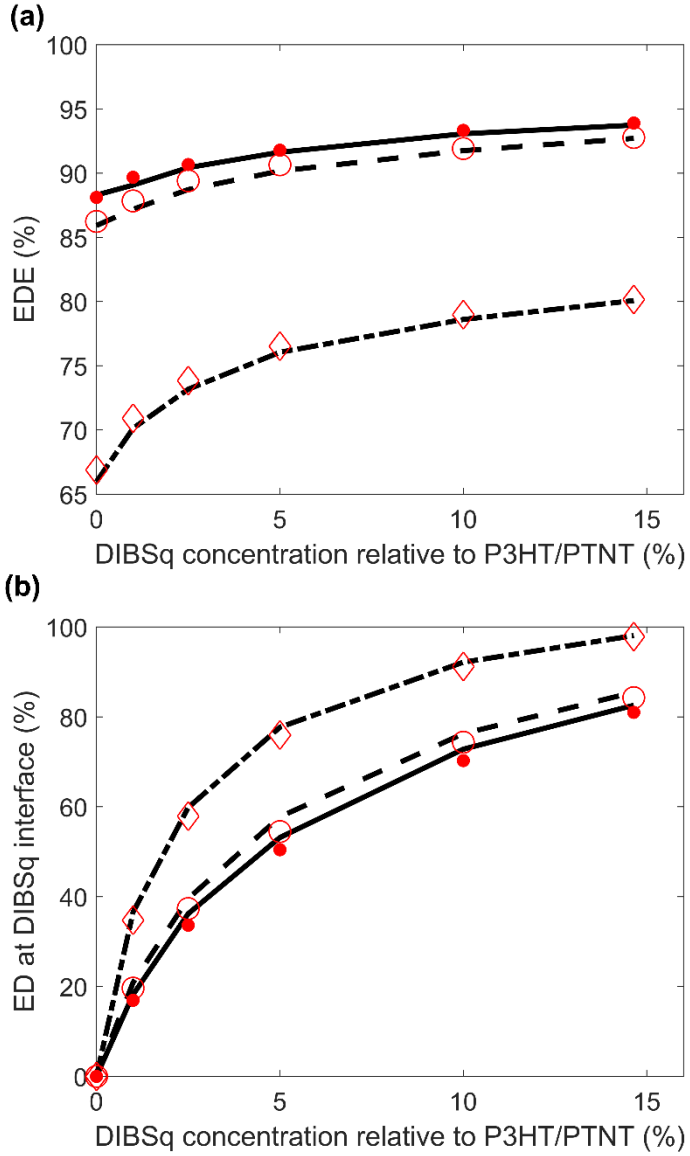

Figure 7. (a) *EDE* as function of DIBSq content for a P3HT:PCBM:DIBSq (black) and PTNT:PCBM:DIBSq (red) BHJ with a feature size of 14 nm (solid line/dots), 15 nm (dashed line/open circles) and 31 nm (dash-dot line/diamonds). The number of excitons that dissociated at the DIBSq interface is also shown as a function of DIBSq content in (b).

As such, adding more than 5% DIBSq is unlikely to further improve the overall power conversion efficiency of P3HT:PCBM:DIBSq BHJ structures, especially if it causes some DIBSq to enter the PCBM or P3HT domains whereupon it acts to trap charges. Indeed, while improved

experimental power conversion efficiencies are seen for all DIBSq concentrations up to 5% (no data is available for higher concentrations due to the low solubility limit of DIBSq), the optimal DIBSq concentration is observed to be <5% [8,19]. In order to determine the role of energy cascades in ternary OPV blends, the behaviour of PTNT:PCBM:DIBSq in the KMC model was also examined. PTNT is a high performance alternative to P3HT[25], but its electronic energy levels are not aligned to form a cascade structure; thus eliminating one energy level offset. Figure 6(b) shows that an exciton in DIBSq does not dissociate at the PTNT interface, but may allow for free (unbound) hole transfer. In the KMC simulations for PTNT:PCBM:DIBSq, the dissociation probability associated with the DIBSq side of the PTNT:DIBSq interface was set to 0 %. Surprisingly, the results in Figure 7(a) show that there is no loss in *EDE* for the PTNT:PCBM:DIBSq blend (compared to P3HT:PCBM:DIBSq) despite not having a cascade energy structure. Even though excitons in DIBSq cannot dissociate at the PTNT interface, they can efficiently dissociate at the PCBM interface; demonstrating that an energy level offset is not required at all interfaces. By moving all excitons to one interface, high V_{OC} can be achieved in ternary devices (as high as in equivalent binary devices) with the benefit of increased light absorption. This result shows that energy level cascades are not required to produce an efficient ternary BHJ device. Rather, the location of DIBSq, or more generally the infra-red absorber, and the energy transfer efficiency to the infra-red absorber are crucial. Figure 7(b) shows that exciton dissociation at the DIBSq interfaces, for both the P3HT:PCBM:DIBSq and PTNT:PCBM:DIBSq blends, does not linearly increase with DIBSq content. Due to long range energy transfer, DIBSq sites are able to harvest excitons from a relatively large volume of the surrounding P3HT (or PTNT) and to a lesser extent PCBM sites. Since the Förster radius for energy transfer from P3HT (or PTNT) to DIBSq is larger than from P3HT to P3HT (or PTNT to PTNT), excitons preferentially move to DIBSq sites, which are located at interfaces that facilitate exciton dissociation thus leading to an improvement in *EDE*. Consequently, a small amount of DIBSq leads to a significant improvement in *EDE*. Two neighbouring DIBSq sites do not harvest twice the amount of excitons from its surroundings, because energy transfer to these two DIBSq sites compete with

each other. More generally, increasing the DIBSq content increases exciton harvesting by DIBSq with a diminishing rate. As a result, the *EDE* is also observed to improve with a diminishing rate. Astonishingly, with a feature size of 31 nm, only 10 % DIBSq is required to force 92 % of all excitons to dissociate at a DIBSq interface. In other words, by controlling where the DIBSq is located one can control where the majority of excitons dissociate.

While the increase in *EDE* with the addition of DIBSq is significant for larger feature sizes (Figure 7 (a)), the ability to control at which interface the excitons dissociate is potentially the most interesting result as it opens up a new way to reduce the energy losses associated with charge separation in ternary organic solar cells. In binary organic solar cells, both a $LUMO_{donor} - LUMO_{acceptor}$ offset and a $HOMO_{donor} - HOMO_{acceptor}$ offset are required to dissociate excitons in both the donor and acceptor moieties. Assuming 0.3 eV is required to dissociate excitons, an overall energy loss of 0.6 eV ($LUMO_{donor} - LUMO_{acceptor}$ offset + $HOMO_{donor} - HOMO_{acceptor}$ offset) is required to achieve high quantum efficiencies. Ternary blends with a cascade structure have six energy level offsets, each introducing an energy loss. Consequently, the V_{OC} in ternary devices are often seen to have a lower V_{OC} compared to the binary equivalent[41], which counteracts the benefit of improved light absorption. However, if energy transfer is utilised to move all excitons to one particular interface, only a single energy level offset is required to dissociate all excitons efficiently. This approach to increasing the V_{OC} is not only applicable to ternary polymer BHJ systems, but also planar structures and small molecules such as rubrene, other squaraines and various acenes for which high device efficiency and/or efficient energy transfer has already been demonstrated[35,42–44].

In BHJ devices, an exciton must dissociate at an interface into its constituent charge carriers, and then those charge carriers must be collected at the electrodes to produce current. As such, the overall power conversion efficiency depends both on the *EDE* and the charge collection efficiency (*CCE*)[16]. Smaller feature sizes have better *EDEs* due to the shorter distances to an interface, but worse *CCEs* as the electrons and holes must navigate an increasingly complex morphology to reach the electrodes. The opposite is true for larger feature size. It has been previously found that this trade-off

means that the best PCEs are produced by moderate feature sizes which balance the *EDE* and *CCE* [16]. Two ways to obtain better PCE in OPV would be to take a large feature size with a naturally good *CCE* and find a way to improve the naturally poor *EDE*, or vice versa for small feature size. The effect of DIBSq in BHJ structures falls into the former category, as the large Förster radius from P3HT and PTNT to DIBSq allows excitons to make large hops directly to the interface. We suggest that the addition of DIBSq to real P3HT:PCBM or PTNT:PCBM BHJ devices helps increase the *PCE* of these devices with further improvements to be expected when optimised for a larger feature size compared to the binary equivalent structure. In other words, the optimum annealing conditions are likely to change upon the addition of DIBSq.

4. Conclusion

In summary, we have determined the energy transfer parameters for P3HT, PCBM, PTNT and DIBSq through spectroscopic measurements and assessed the necessity for accurately modelling hetero-energy transfer in binary BHJ systems to calculate the exciton dissociation efficiency. In principle, hetero-energy transfer must be taken into account to avoid over- or underestimation of the *EDE*. However, for systems where hole transfer and electron transfer across the interface are the same, such as P3HT:PCBM, accurate *EDEs* are calculated even when hetero-energy transfer is completely ignored. Hetero-energy transfer causes *EDE* to be insensitive to the exciton dissociation probability at the energy donor side of the interface. As such, exciton dissociation can still be efficient even if one of the energy level offsets (HOMOdonor – HOMOacceptor or LUMOdonor – LUMOacceptor) is smaller than the exciton binding energy. The broad absorption range of PCBM means that energy transfer to PCBM is possible from various donor materials, which may partially explain the seemingly universal compatibility of PCBM with many donor materials in OPV devices.

Energy transfer is a crucial part of the photoconversion mechanism in ternary bulk heterojunction solar cells. We have shown that energy transfer relaxes the electronic energy level requirements of the three components, because it enables non-cascade structures to still dissociate

excitons efficiently. For example, a ternary system such as PTNT:PCBM:DIBSq is expected to perform well despite the poor exciton dissociation efficiency at the DIBSq:PTNT interface. More importantly, by eliminating the unnecessary energy offsets the loss in V_{OC}, often seen in ternary devices, can be eliminated entirely while still enjoying the benefit of improved light absorption (and thus J_{SC}).

It is important for the infra-red sensitiser to be located at the electron donor/acceptor interface to prevent charge traps and to preferentially transport excitons to an interface where dissociation occurs efficiently. Only small amounts of DIBSq are required to cover a large fraction of the P3HT:PCBM interface. Our results suggest that the available interface area in a BHJ structure may limit the optimum concentration of the infra-red sensitizer. The solubility limit of DIBSq is low, which limits how much DIBSq can be added to a P3HT:PCBM blend. Fortunately, only small quantities of DIBSq (<5 %) are required to cause substantial improvements in *EDE* due to long-range energy transfer. Long-range energy transfer from P3HT to DIBSq not only improves *PCE* by enhancing *EDE*, but also allows for the use of larger feature sizes without significant loss in *EDE*, which is beneficial for charge collection. As such, the optimum feature size of P3HT:PCBM:DIBSq BHJ systems are likely to be larger compared to P3HT:PCBM binary systems.

Supporting Information. Absorbance spectra of DIBSq in solution, DIBSq as a solid film and a film of P3HT:PCBM:DIBSq before and after annealing.

Acknowledgements

ARENA is acknowledged for financial support (KF). This work was performed in part at the Materials and NSW node of the Australian National Fabrication Facility, which is a company established under the National Collaborative Research Infrastructure Strategy to provide nano and microfabrication facilities for Australia's researchers. JMC and ABW acknowledge funding from UK Engineering and Physical Sciences Research Council grants EP/L01551X/1 (Centre for Doctoral Training in New and

Sustainable PV) and EP/J017361/1 (SuperSolar Solar Energy Hub). JMC acknowledges funding from CSIRO.

References

(1) Chiechi, R. C.; Havenith, R. W. a.; Hummelen, J. C.; Koster, L. J. A.; Loi, M. a. Modern Plastic Solar Cells: Materials, Mechanisms and Modeling. *Mater. Today* **2013**, *16* (7-8), 281–289.

(2) Günes, S.; Neugebauer, H.; Sariciftci, N. S. Conjugated Polymer-Based Organic Solar Cells. *Chem. Rev.* **2007**, *107* (4), 1324–1338.

(3) Veldman, D.; Meskers, S. C. J.; Janssen, R. A. J. The Energy of Charge-Transfer States in Electron Donor-Acceptor Blends: Insight into the Energy Losses in Organic Solar Cells. *Adv. Funct. Mater.* **2009**, *19* (12), 1939–1948.

(4) Li, W.; Hendriks, K. H.; Furlan, A.; Wienk, M. M.; Janssen, R. A. J. High Quantum Efficiencies in Polymer Solar Cells at Energy Losses below 0.6 eV. *J. Am. Chem. Soc.* **2015**, *137* (6), 2231–2234.

(5) Janssen, R. A. J.; Nelson, J. Factors Limiting Device Efficiency in Organic Photovoltaics. *Adv. Mater.* **2013**, *25* (13), 1847–1858.

(6) Yao, K.; Xu, Y.-X.; Li, F.; Wang, X.; Zhou, L. A Simple and Universal Method to Increase Light Absorption in Ternary Blend Polymer Solar Cells Based on Ladder-Type Polymers. *Adv. Opt. Mater.* **2015**, *3* (3), 321–327.

(7) Lu, L.; Xu, T.; Chen, W.; Landry, E. S.; Yu, L. Ternary Blend Polymer Solar Cells with Enhanced Power Conversion Efficiency. *Nat. Photonics* **2014**, *8* (9), 716–722.

(8) Huang, J.-S.; Goh, T.; Li, X.; Sfeir, M. Y.; Bielinski, E. a.; Tomasulo, S.; Lee, M. L.; Hazari, N.; Taylor, A. D. Polymer Bulk Heterojunction Solar Cells Employing Förster Resonance Energy Transfer. *Nat. Photonics* **2013**, *7* (6), 479–485.

(9) Cnops, K.; Rand, B. P.; Cheyns, D.; Verreet, B.; Empl, M. a; Heremans, P. 8.4% Efficient

Fullerene-Free Organic Solar Cells Exploiting Long-Range Exciton Energy Transfer. *Nat. Commun.* **2014**, *5*, 3406.

(10) Ameri, T.; Khoram, P.; Min, J.; Brabec, C. J. Organic Ternary Solar Cells: A Review. *Adv. Mater.* **2013**, *25* (31), 4245–4266.

(11) Honda, S.; Ohkita, H.; Benten, H.; Ito, S. Multi-Colored Dye Sensitization of Polymer/fullerene Bulk Heterojunction Solar Cells. *Chem. Commun.* **2010**, *46* (35), 6596–6598.

(12) Honda, S.; Ohkita, H.; Benten, H.; Ito, S. Selective Dye Loading at the Heterojunction in Polymer/Fullerene Solar Cells. *Adv. Energy Mater.* **2011**, *1* (4), 588–598.

(13) Feron, K.; Zhou, X.; Belcher, W. J.; Fell, C. J.; Dastoor, P. C. A Dynamic Monte Carlo Study of Anomalous Current Voltage Behaviour in Organic Solar Cells. *J. Appl. Phys.* **2014**, *116* (21), 214509.

(14) Feron, K.; Zhou, X.; Belcher, W. J.; Dastoor, P. C. Exciton Transport in Organic Semiconductors: Förster Resonance Energy Transfer Compared with a Simple Random Walk. *J. Appl. Phys.* **2012**, *111* (4), 044510.

(15) Feron, K.; Fell, C. J.; Rozanski, L. J.; Gong, B. B.; Nicolaidis, N.; Belcher, W. J.; Zhou, X.; Sesa, E.; King, B. V.; Dastoor, P. C. Towards the Development of a Virtual Organic Solar Cell: An Experimental and Dynamic Monte Carlo Study of the Role of Charge Blocking Layers and Active Layer Thickness. *Appl. Phys. Lett.* **2012**, *101* (19), 193306.

(16) Watkins, P. K.; Walker, A. B.; Verschoor, G. L. B. Dynamical Monte Carlo Modelling of Organic Solar Cells: The Dependence of Internal Quantum Efficiency on Morphology. *Nano Lett.* **2005**, *5* (9), 1814–1818.

(17) Kimber, R. G. E.; Walker, A. B.; Schröder-Turk, G. E.; Cleaver, D. J. Bicontinuous Minimal Surface Nanostructures for Polymer Blend Solar Cells. *Phys. Chem. Chem. Phys.* **2010**, *12* (4), 844–851.

(18) Feron, K.; Belcher, W. J.; Fell, C. J.; Dastoor, P. C. Organic Solar Cells: Understanding the

Role of Förster Resonance Energy Transfer. *Int. J. Mol. Sci.* **2012**, *13* (12), 17019–17047.

(19) An, Q.; Zhang, F.; Li, L.; Wang, J.; Zhang, J.; Zhou, L.; Tang, W. Improved Efficiency of Bulk Heterojunction Polymer Solar Cells by Doping Low-Bandgap Small Molecules. *ACS Appl. Mater. Interfaces* **2014**, *6* (9), 6537–6544.

(20) Athanasopoulos, S.; Emelianova, E. V.; Walker, A. B.; Beljonne, D. Exciton Diffusion in Energetically Disordered Organic Materials. *Phys. Rev. B* **2009**, *80* (19), 195209.

(21) Meng, L.; Shang, Y.; Li, Q.; Li, Y.; Zhan, X.; Shuai, Z.; Kimber, R. G. E.; Walker, A. B. Dynamic Monte Carlo Simulation for Highly Efficient Polymer Blend Photovoltaics. *J. Phys. Chem. B* **2010**, *114* (1), 36–41.

(22) Förster, T. Zwischenmolekulare Energiewanderung Und Fluoreszenz. *Ann. Phys.* **1948**, *437* (1-2), 55–75.

(23) Loura, L. M. S. Simple Estimation of Förster Resonance Energy Transfer (FRET) Orientation Factor Distribution in Membranes. *Int. J. Mol. Sci.* **2012**, *13*, 15252–15270.

(24) Gillespie, D. T. A General Method for Numerically Simulating the Stochastic Time Evolution of Coupled Chemical Reactions. *J. Comput. Phys.* **1976**, *22* (4), 403–434.

(25) Kroon, R.; Diaz de Zerio Mendaza, A.; Himmelberger, S.; Bergqvist, J.; Bäcke, O.; Faria, G. C.; Gao, F.; Obaid, A.; Zhuang, W.; Gedefaw, D.; Olsson, E.; Inganäs, O.; Salleo, A.; Müller, C.; Andersson, M. R. A New Tetracyclic Lactam Building Block for Thick, Broad-Bandgap Photovoltaics. *J. Am. Chem. Soc.* **2014**, *136* (33), 11578–11581.

(26) Brouwer, A. M. Standards for Photoluminescence Quantum Yield Measurements in Solution (IUPAC Technical Report). *Pure Appl. Chem.* **2011**, *83* (12), 2213–2228.

(27) Ma, W.; Yang, C.; Gong, X.; Lee, K.; Heeger, A. J. Thermally Stable, Efficient Polymer Solar Cells with Nanoscale Control of the Interpenetrating Network Morphology. *Adv. Funct. Mater.* **2005**, *15* (10), 1617–1622.

(28) Bässler, H. Charge Transport in Disordered Organic Photoconductors a Monte Carlo Simulation Study. *Phys. Status Solidi B* **1993**, *175* (1), 15–56.

(29) Scheidler, M.; Lemmer, U.; Kersting, R.; Karg, S.; Riess, W.; Cleve, B.; Mahrt, R. F.; Kurz, H.; Bässler, H.; Göbel, E. O.; Thomas, P. Monte Carlo Study of Picosecond Exciton Relaxation and Dissociation in Poly(phenylenevinylene). *Phys. Rev. B* **1996**, *54* (8), 5536–5544.

(30) Shaw, P. E.; Ruseckas, A.; Samuel, I. D. W. Exciton Diffusion Measurements in Poly(3-Hexylthiophene). *Adv. Mater.* **2008**, *20* (18), 3516–3520.

(31) Wang, H.; He, Y.; Li, Y.; Su, H. Photophysical and Electronic Properties of Five PCBM-like C 60 Derivatives: Spectral and Quantum Chemical View. *J. Phys. Chem. A* **2012**, *116* (1), 255–262.

(32) Cook, S.; Furube, A.; Katoh, R.; Han, L. Estimate of Singlet Diffusion Lengths in PCBM Films by Time-Resolved Emission Studies. *Chem. Phys. Lett.* **2009**, *478* (1-3), 33–36.

(33) *L in PTNT Was Assumed to Be Similar to P3HT, Because the Optimum Feature Size Is Similar.*

(34) *Lifetime Was Assumed to Be the Same as P3HT.*

(35) Wei, G.; Xiao, X.; Wang, S.; Sun, K.; Bergemann, K. J.; Thompson, M. E.; Forrest, S. R. Functionalized Squaraine Donors for Nanocrystalline Organic Photovoltaics. *ACS Nano* **2012**, *6* (1), 972–978.

(36) Lloyd, M. T.; Lim, Y.-F.; Malliaras, G. G. Two-Step Exciton Dissociation in poly(3-Hexylthiophene)/fullerene Heterojunctions. *Appl. Phys. Lett.* **2008**, *92* (14), 143308.

(37) Coffey, D. C.; Larson, B. W.; Hains, A. W.; Whitaker, J. B.; Kopidakis, N.; Boltalina, O. V.; Strauss, S. H.; Rumbles, G. An Optimal Driving Force for Converting Excitons into Free Carriers in Excitonic Solar Cells. *J. Phys. Chem. C* **2012**, *116* (16), 8916–8923.

(38) Cook, S.; Katoh, R.; Furube, a. Exciton Splitting in Nanoscale Phase-Separated Polythiophene:Fullerene Solar Cell Blends. *J. Nanoelectron. Optoelectron.* **2010**, *5* (2), 115–119.

(39) Piris, J.; Dykstra, T. E.; Bakulin, A. a.; van Loosdrecht, P. H. M.; Knulst, W.; Trinh, M. T.;

Schins, J. M.; Siebbeles, L. D. A. Photogeneration and Ultrafast Dynamics of Excitons and Charges in P3HT/PCBM Blends. *J. Phys. Chem. C* **2009**, *113* (32), 14500–14506.

(40) Goh, T.; Huang, J.-S.; Bielinski, E. a.; Thompson, B. a.; Tomasulo, S.; Lee, M. L.; Sfeir, M. Y.; Hazari, N.; Taylor, A. D. Coevaporated Bisquaraine Inverted Solar Cells: Enhancement Due to Energy Transfer and Open Circuit Voltage Control. *ACS Photonics* **2015**, *2* (1), 86–95.

(41) Khlyabich, P. P.; Rudenko, A. E.; Thompson, B. C.; Loo, Y.-L. Structural Origins for Tunable Open-Circuit Voltage in Ternary-Blend Organic Solar Cells. *Adv. Funct. Mater.* **2015**, *25* (34), 5557–5563.

(42) Griffith, O. L.; Forrest, S. R. Exciton Management in Organic Photovoltaic Multidonor Energy Cascades. *Nano Lett.* **2014**, *14* (5), 2353–2358.

(43) Schlenker, C. W.; Barlier, V. S.; Chin, S. W.; Whited, M. T.; McAnally, R. E.; Forrest, S. R.; Thompson, M. E. Cascade Organic Solar Cells. *Chem. Mater.* **2011**, *23* (18), 4132–4140.

(44) Yang, F.; Lunt, R. R.; Forrest, S. R. Simultaneous Heterojunction Organic Solar Cells with Broad Spectral Sensitivity. *Appl. Phys. Lett.* **2008**, *92* (5), 053310.